Catalysis at single-crystal Pt(110) surfaces: Global coupling and standing waves

Herbert Levine and Xiaoqin Zou
Department of Physics and Institute for Nonlinear Science, University of California, San Diego, La Jolla, California 92093
(Received 9 November 1992)

Recently various types of spatiotemporal concentration patterns have been observed in experimental studies of catalysis on single-crystal surfaces. One of the most interesting phenomena among these is the standing-wave pattern which has been seen in $CO+O_2 \rightarrow CO_2$ on Pt(110). A kinetic model involving surface reconstruction has been proposed for this system by Eiswirth, Krischer, and Ertl [Appl. Phys. A **51**, 79 (1990)]. Here, we add spatial-coupling terms due both to CO diffusion and to global gas-phase fluctuations and we study the possible wave patterns in this set of reaction-diffusion equations. We argue that the standing waves may be due to a self-induced parametric driving mechanism. Our analytical results as well as our numerical simulations are qualitatively consistent with the experimental findings.

PACS number(s): 05.70.Ln, 82.20.Mj, 82.65.−i, 47.20.Ky

I. INTRODUCTION

The study of chemical spatiotemporal patterns has attracted considerable interest during the past several years. Typically, these far-from-equilibrium processes are described by nonlinear reaction-diffusion differential equations. Some striking examples include the Belusov-Zhabotinskii (BZ) reaction [1], CO oxidation over single-crystal [2] and polycrystalline [3] catalysts, and Dictyoselium aggregation [4]. Much experimental and theoretical effort has been devoted to the study of traveling waves and rotating spirals in the BZ reaction [5,6]. There has also been some work devoted towards understanding trigger waves in catalytic oxidation [7–9]. In both of these cases, the mathematical analysis has been based on the assumptions that there exist one slowly reacting species and one or more rapidly reacting species; calculations are carried out by using singular perturbation theory in the comoving frame of reference.

Recently, Ertl and co-workers have observed a large variety of new spatiotemporal patterns associated with the oscillatory oxidation of CO on a Pt(110) surface; this work was accomplished by employing the technique of the photoemission electron microscopy (PEEM) [10–13] to obtain the necessary spatial resolution. In addition to the expected traveling waves and rotating spirals, standing waves and even solitons are obtained under certain experimental conditions. For the latter two spatial patterns one cannot transform the partial differential equations into ordinary differential equations by introducing a comoving frame. We must instead resort to an alternative methodology.

The purpose of this paper is to make a step towards understanding standing-wave patterns in the aforementioned problem. We shall start by reviewing the results of the Ertl *et al.* experiments. Next, we introduce CO diffusion as well as global-coupling terms to the three-variable reaction kinetics scheme of Eiswirth, Krischer, and Ertl [14,15] (EKE) so as to model spatiotemporal patterns. The global coupling is motivated by some specific experimental observations concerning CO partial-pressure oscillations. Next, we use standard bifurcation-theory methods to derive coupled small-amplitude equations valid near the Hopf bifurcation of the reaction-diffusion system. The solutions of these coupled complex Ginzburg-Landau equations can be in the form of standing-wave patterns. Finally, in order to check the analytical results, we will describe some limited simulation studies of our model. Some of our results have appeared in preliminary form elsewhere [16].

One interesting result which emerges from our analysis relates to the possible existence of a codimension-two point at which $q=0$ and $q\neq 0$ simultaneously undergo Hopf bifurcations with similar frequencies. Mathematically this is possible only in the presence of certain types of global coupling. The coupled set of amplitude equations near this point predicts the presence of standing waves modulated by an overall (global) oscillation. In fact, one does observe these modulated waves even without global coupling due to the presence of strong-mode interactions. This will be demonstrated by direct simulation of our model.

II. EXPERIMENTAL RESULTS AND THEORETICAL MODEL

As mentioned above, several experimental studies of CO oxidation on Pt(110) have been performed by Ertl's group using the PEEM technique [10]. They observed that at high-enough temperature, rapid regular oscillations are associated with standing waves. These waves reflect rapidly varying (in time) surface concentrations of the reacting species with additional spatial modulations. These spatial structures are actually quite complex due to the presence of dislocations which destroy the one-dimensional nature of the wave; as the system evolves in time, these dislocations may increase in density, and may even exhibit varying orientations so that they eventually

1063-651X/93/48(1)/50(15)/$06.00

intersect each other. One result of this is the formation of rhombic-shaped spatiotemporal patterns. In this paper, however, we will restrict ourselves to the strictly one-dimensional case as a first step towards understanding these phenomena.

According to earlier experimental results [17], the mechanism underlying the occurrence of kinetic oscillations is as follows. First, the clean Pt(110) surface exhibits a 1×2 missing-row reconstruction from a 1×1-structure [13]. This leads to the existence of two branches of the reaction rate as a function of the CO and O coverages. The high-reaction-rate branch is associated with the oxygen-covered 1×2 surface, while the low one belongs to a CO-covered 1×1 surface. Successive transitions between the two branches lead to the kinetic oscillations. The temperature at which oscillations are detected in the 10^{-5} and 10^{-4} Torr pressure regime ranges from 440 to 600 K.

It is worth noting that the width in parameter space over which oscillations exist is rather narrow. This is in contrast to the same reaction over Pt(100) where P_{CO} can be varied over a wide region for a given temperature and given P_{O_2} without leaving the oscillatory region. The narrowness of this region leads to an observed high sensitivity of the reactions on Pt(110) towards partial-pressure variations. This in turn leads [18] to the importance of feedback effects through the gas phase as the pressure is modulated by the reaction. Because of rapid mixing of the gas, this gas-phase coupling is global in nature. This might be expected to be important for possible macroscopic spatial patterns and could lead, for example, to synchronized behavior of the whole surface. One indication that this may be occurring is the lack of propagating-wave phenomena at high-enough temperatures.

In addition, material can diffuse on the surface. According to Ref. [2], the diffusion constant of CO on Pt(110) $D\sim10^{-4}\ \mathrm{mm^2\,s^{-1}}$, while the oxygen surface diffusion is very small and can therefore be ignored.

In summary, two dominant factors should account for the standing-wave patterns on Pt(110) at high temperatures. The phase transition between the reconstructed (1×2) phase and the bulk (1×1) phase gives rise to the kinetic oscillations and the spatial coupling due to both CO diffusion and especially the aforementioned gas-phase coupling are responsible for the patterns. We need to mention that the influence of the facet formation has been ignored here since no noticeable facets can be observed at high temperatures.

Based on this set of experiments, Eiswirth, Krischer, and Ertl have suggested a mathematical reaction model incorporating the proposed surface-reconstruction model [14,15],

$$\begin{aligned}\dot{c}&=f_1(c,o,a)\ ,\\ \dot{o}&=f_2(c,o,a)\ ,\\ \dot{a}&=f_3(c,o,a)\ ,\end{aligned}\tag{1}$$

where

$$f_1=k_c s_c\left[1-\left[\frac{c}{c_s}\right]^3\right]-k_4 c-k_3 co\ ,$$

$$f_2=k_o s_o\left[1-\frac{c}{c_s}-\frac{o}{o_s}\right]^2-k_3 co\ ,$$

$$f_3=\begin{cases}-k_5 a & \text{if } c\le c_1\\ k_5\left[\sum_{i=0}^{3} r_i c^i-a\right] & \text{if } c_1<c<c_2\\ k_5(1-a) & \text{if } c\ge c_2.\end{cases}$$

Here c and o are the coverages of CO and O on the Pt surface; c_s and o_s are the respective saturation coverages; s_c and s_o are the sticking coefficients; k_c and k_o are the rates at which molecules hit the surface; k_3 and k_4 are, respectively, the rate constants of the Langmuir-Hinshelwood reaction which actually forms the CO_2 (which is immediately released) and CO desorption. In the small temperature range of interest, the rate constants k_c and k_o are, as expected, found to be independent of temperature and thus $k_c=k_1P_{\mathrm{CO}}$, $k_o=k_2P_{\mathrm{O}_2}$. k_3 and k_4 vary with temperature as $k_i(T)=k_i^0\exp(-E_i/RT)$. Finally, a is the fraction of the surface with 1×1 structure. c_1 (c_2) are the critical CO coverages at which the elimination (completion) of the reconstruction occurs; for concentrations between these limits, a four-term polynomial in c was chosen to give a monotonic and differentiable function varying from 0 to 1. We will take $s_c=1$, but $s_o=as_{o_1}+(1-a)s_{o_2}$ since the oxygen-sticking probability is different on the two different surface phases. All parameters in the above equations are listed in Table I, taken from Ref. [15].

As mentioned above, we will modify the above equations by taking into consideration the global gas-phase coupling as well as the diffusion term. This results in the following equations:

$$\begin{aligned}\dot{c}&=F_1(c,o,a)+D\frac{\partial^2 c}{\partial x^2}\ ,\\ \dot{o}&=F_2(c,o,a)\ ,\\ \dot{a}&=F_3(c,o,a)\ ,\end{aligned}\tag{2}$$

where

$$F_1=k_1P_{\mathrm{CO}}(1+\alpha'\bar{c}-\alpha\bar{o})s_c\left[1-\left[\frac{c}{c_s}\right]^3\right]-k_4c-k_3co\ ,$$

$$F_2=k_2P_{\mathrm{O}_2}(1+\beta'\bar{o}-\beta\bar{c})s_o\left[1-\frac{c}{c_s}-\frac{o}{o_s}\right]^2-k_3co\ ,$$

$$F_3=f_3\ ,$$

$$\bar{c}\equiv\frac{1}{L}\int c\,dx,\quad \bar{o}\equiv\frac{1}{L}\int o\,dx\ .$$

We have here used the assumption that the partial pressures in the gas phase are proportional to the average coverages on the surface. This idea is based on the experimentally measured oscillations in the partial pressure to-

TABLE I. Parameters for the EKE reaction; here $k_i = k_i^0 e^{-E_i/RT}$ for $i = 3,4,5$.

Quantity	Description	Value	
	CO		
k_1	Flux	4.18×10^5 s^{-1}Torr^{-1}	
s_c	Sticking coefficient	1	
c_s	Saturation coverage	1	
	O_2		
k_2	Flux	7.81×10^5 s^{-1}Torr^{-1}	
s_{o_1}	Sticking coefficient on 1×1	0.6	
s_{o_2}	Sticking coefficient on rec	0.4	
o_s	Saturation coverage	0.8	
	Rates		
k_3	Reaction	$k_3^0 = 3\times10^6$ s^{-1}	$E_3 = 10$ kcal/mol
k_4	CO desorption	$k_4^0 = 2\times10^{16}$ s^{-1}	$E_4 = 38$ kcal/mol
k_5	Phase transition	$k_5^0 = 10^2$ s^{-1}	$E_4 = 7$ kcal/mol
r_i	Coefficients for phase transition	$r_3 = -1/0.0135$	$r_2 = -1.05r_3$
		$r_1 = 0.3r_3$	$r_0 = -0.026r_3$
c_i	Critical coverages for phase transition	$c_1 = 0.2$	$c_2 = 0.5$

gether with the fact that rapid mixing causes instantaneous equilibration in the gas phase. That is, the gas pressure at any fixed point reacts to the change in total concentration, since horizontal gradients in the gas disappear on a much faster time scale. Also, the global-coupling coefficients α,α' are positive and β,β' are negative as a consequence of asymmetric inhibition of adsorption [18]. More specifically, variations of the partial pressures are in phase with CO coverage and out of phase with O coverage because a CO-covered surface blocks the adsorption of both CO and O_2 but not vice versa. An O-covered surface blocks the adsorption of O_2 but not CO.

In this paper, we will analyze the above system as to the possible nonlinear states that can exist near the occurrence of Hopf bifurcations of the steady-state solution. Our most interesting results will come about by assuming that the global-coupling coefficients have been chosen so as to allow for the existence of a degenerate codimension two bifurcation. Near this point, two traveling-wave amplitudes (at $\pm q$) will couple to a global oscillation. It is important to realize that the results which emerge from the amplitude-equation analysis close to the codimension-two point may actually describe the nonlinear behavior of the system even if the coefficients α, α', β, β' of the actual system do not admit an actual codimension-two point. In effect, we will argue that the physical mechanisms underlying the observed standing-wave behavior is most easily described mathematically by expanding about a (possibly) unphysical point in parameter space. Numerical evidence for this will be given later.

III. BIFURCATION ANALYSIS

As originally shown in Ref. [14], the reaction kinetic scheme given by Eqs. (2) exhibits a Hopf bifurcation. Our first goal will be to extend the calculation of this instability to modes with finite spatial wave vector q. Then, we will use well-established methods to derive coupled amplitude equations governing the competition between traveling waves and standing waves. We will discover that standing waves are indeed preferred (at sufficiently large q), in agreement with their experimental occurrence. We will perform these calculations first without the global couplings and then with the full model; this will serve to explicitly elucidate the role of the global couplings.

A. Hopf bifurcation

To find the location of the Hopf bifurcation, we must solve for the steady-state solutions first and then calculate their stability. Without the global couplings, the steady-state solutions (c_0,o_0,a_0) are given by $\dot{c}=\dot{o}=\dot{a}=\partial^2 c/\partial x^2=0$, viz.,

$$f_i(c_0,o_0,a_0)=0, \quad i=1,2,3 \ . \tag{3}$$

Define vectors $\mathbf{Y}\equiv(c,o,a)$ and $\mathbf{Y}_0\equiv(c_0,o_0,a_0)$. Then define the concentration deviation $\mathbf{u}=\mathbf{Y}-\mathbf{Y}_0$. If the spatial dependence of the perturbation has a sinusoidal form $\cos(qx)$, the linear approximation to the system near an equilibrium state is therefore

$$\frac{d\mathbf{u}}{dt}=\mathbf{L}\mathbf{u}-q^2\mathbf{D}\mathbf{u} \ , \tag{4}$$

where $L_{ij}=\partial f_i(\mathbf{Y}_0)/\partial Y_{0j}$, $D_{ij}=1$ if $i=j=1$ or 0 otherwise.

The Hopf bifurcation occurs at those points on the P_{CO}-P_{O_2} phase plane when $(\mathbf{L}-q^2\mathbf{D})$ has a pair of pure imaginary conjugate eigenvalues with all other eigenvalues having a nonzero real part. For $q=0$ case, the Hopf-bifurcation contour has already been calculated in Ref. [15], namely, the contour of region 7 in Fig. 1 of that paper. When q is increased, the Hopf-bifurcation contour will shrink and will finally disappear for a maximum value of q. This nested structure is illustrated in Fig. 1.

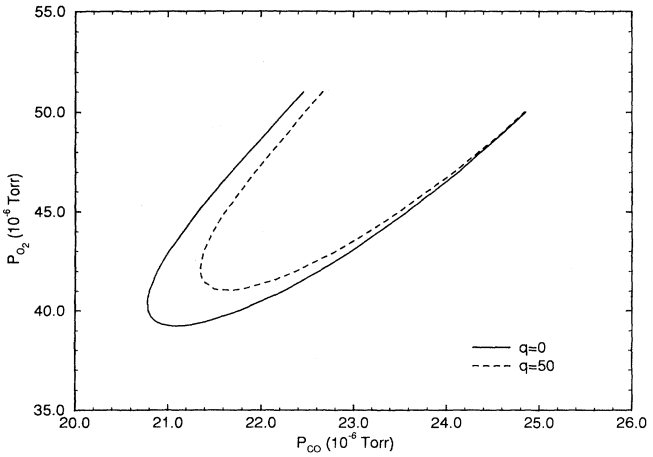

FIG. 1. Contours of the Hopf bifurcation without any global couplings. Temperature is always chosen to be 540 K in this paper.

B. Amplitude equations without global coupling

Next we will consider expanding the concentration fields near the Hopf-bifurcation point. Again, we will first not take into account the global coupling. By expanding the dynamic equation (2) in a Taylor series in $\mathbf{u}$, we obtain [19,20]

$$\frac{\partial \mathbf{u}}{\partial t}=\mathbf{D}\partial_x^2\mathbf{u}+\mathbf{L}\mathbf{u}+\mathbf{M}\mathbf{u}\mathbf{u}+\mathbf{N}\mathbf{u}\mathbf{u}\mathbf{u}+\cdots . \tag{5}$$

Here the abbreviations **Muu** and **Nuuu**, etc. indicate vectors whose ith components are given by

$$(\mathbf{Muu})_i=\sum_{j,k}\frac{1}{2!}\frac{\partial^2 f_i(\mathbf{Y}_0)}{\partial Y_{0j}\partial Y_{0k}}u_j u_k ,$$

$$(\mathbf{Nuuu})_i=\sum_{j,k,l}\frac{1}{3!}\frac{\partial^3 f_i(\mathbf{Y}_0)}{\partial Y_{0j}\partial Y_{0k}\partial Y_{0l}}u_j u_k u_l ,$$

and higher-order terms in $\mathbf{u}$ may be expressed similarly. We shall later use quantities **Muv** and **Nuvw** for different vectors $\mathbf{u}$, $\mathbf{v}$, and $\mathbf{w}$, and their definitions may be understood as an obvious extension of the above. For simplicity, we will fix P_{O_2} and only consider changes in P_{CO} to move us away from the bifurcation point.

Assume therefore that (P_{CO0},P_{O_20}) is on the Hopf-bifurcation line. Then near criticality, the matrix $\mathbf{L}$ may be expanded in powers of ΔP_{CO},

$$\mathbf{L}=\mathbf{L}_0+\Delta P_{CO}\mathbf{L}_1+(\Delta P_{CO})^2\mathbf{L}_2+\cdots . \tag{6}$$

It is convenient to define a small positive parameter ϵ by $\epsilon^2\chi=\Delta P_{CO}$, where $\chi=\mathrm{sgn}(\Delta P_{CO})$; ϵ is considered to be a measure of the amplitude to lowest order, so that one may assume the expansion

$$\mathbf{u}=\epsilon\mathbf{u}_1+\epsilon^2\mathbf{u}_2+\cdots . \tag{7}$$

The expression in (6) now becomes

$$\mathbf{L}=\mathbf{L}_0+\epsilon^2\chi\mathbf{L}_1+\epsilon^4\mathbf{L}_2+\cdots . \tag{8}$$

Similarly, for the higher-order expansion coefficients in (5), we write symbolically

$$\begin{aligned}\mathbf{M}&=\mathbf{M}_0+\epsilon^2\chi\mathbf{M}_1+\cdots ,\\ \mathbf{N}&=\mathbf{N}_0+\epsilon^2\chi\mathbf{N}_1+\cdots .\end{aligned} \tag{9}$$

To obtain the lowest-order consistency condition in (5), we introduce a scaled time τ via $\tau=\epsilon^2 t$ and regard $\mathbf{u}$ as depending both on t and τ. The time differentiation in (5) is transformed to

$$\frac{d}{dt}\rightarrow\frac{\partial}{\partial t}+\epsilon^2\frac{\partial}{\partial\tau} . \tag{10}$$

Let us first consider the $q=0$ case, viz., the leading term in $\mathbf{u}$ is spatially uniform. Then substituting into (5) gives

$$\begin{aligned}&\left[\frac{\partial}{\partial t}+\epsilon^2\frac{\partial}{\partial\tau}-\mathbf{L}_0-\epsilon^2\chi\mathbf{L}_1-\cdots\right](\epsilon\mathbf{u}_1+\epsilon^2\mathbf{u}_2+\cdots)\\ &\quad=\epsilon^2\mathbf{M}_0\mathbf{u}_1\mathbf{u}_1+\epsilon^3(2\mathbf{M}_0\mathbf{u}_1\mathbf{u}_2+\mathbf{N}_0\mathbf{u}_1\mathbf{u}_1\mathbf{u}_1)+O(\epsilon^4) .\end{aligned} \tag{11}$$

We note in passing that if we were to also consider spatially varying amplitudes, it would be appropriate to characterize the slow space dependence of $\mathbf{u}$ by a scaled coordinate X, defined by $X=\epsilon x$.

Equating the coefficients of different powers of ϵ in (11), we have a set of equations in the form

$$\left[\frac{\partial}{\partial t}-\mathbf{L}_0\right]\mathbf{u}_\nu=\mathbf{B}_\nu,\quad \nu=1,2,3,\ldots . \tag{12}$$

The first few $\mathbf{B}_\nu$'s are

$$\begin{aligned}\mathbf{B}_1&=0 ,\\ \mathbf{B}_2&=\mathbf{M}_0\mathbf{u}_1\mathbf{u}_1 ,\\ \mathbf{B}_3&=-\left[\frac{\partial}{\partial\tau}-\chi\mathbf{L}_1\right]\mathbf{u}_1+2\mathbf{M}_0\mathbf{u}_1\mathbf{u}_2+\mathbf{N}_0\mathbf{u}_1\mathbf{u}_1\mathbf{u}_1 .\end{aligned} \tag{13}$$

In general, the $\mathbf{B}_\nu$'s are functions of the lower-order quantities $\mathbf{u}_{\nu'}$'s ($\nu'<\nu$).

When $\nu=1$, (12) is a homogeneous equation, which simply corresponds to the Hopf bifurcation mentioned above. The solution is in the form

$$\mathbf{u}_1=\mathbf{e}A(\tau,X)e^{i\omega t}+\text{c.c.} , \tag{14}$$

where $i\omega$ and $\mathbf{e}$ are the eigenvalue and the corresponding eigenvector of the linear problem $\mathbf{L}_0\mathbf{e}=i\omega\mathbf{e}$. $A(\tau,X)$ is some complex amplitude yet to be specified.

In order to solve linear inhomogeneous equations (12) with $\nu>2$, we decompose $\mathbf{B}_\nu$ into various harmonics,

$$\mathbf{B}_\nu=\sum_{l=-\infty}^{\infty}\mathbf{B}_\nu^{(l)}e^{il\omega t} .$$

Then the solvability condition will be

$$\mathbf{e}_L\cdot\mathbf{B}_\nu^{(1)}=0 , \tag{15}$$

where $\mathbf{e}_L$ is the left eigenvector of $\mathbf{L}_0$ corresponding to eigenvalue $i\omega$, that is, $\mathbf{e}_L\mathbf{L}_0=i\omega\mathbf{e}_L$. To remove the indeter-

minacy, we can add a supplementary condition that $\mathbf{u}_2$ be orthogonal to $\mathbf{u}_1$, etc.

It is easy to prove that this solvability condition (15) is trivially satisfied for $\nu=2$. So, the equation obeyed by A is given by the solvability condition to third order. $\mathbf{B}_3^{(1)}$ contains not only $\mathbf{u}_1$ but also $\mathbf{u}_2$ which we must first determine. Upon inspection, $\mathbf{u}_2$ has the form

$$\mathbf{u}_2=\mathbf{V}_+A^2e^{2i\omega t}+\mathbf{V}_-A^{*2}e^{-2i\omega t}+\mathbf{V}_0|A|^2 . \tag{16}$$

By substituting this into (12) for $\nu=2$, we can obtain quantities $V_{\pm,0}$ as follows:

$$\begin{aligned}&\mathbf{V}_+=\mathbf{V}_-^*=-(\mathbf{L}_0-2i\omega)^{-1}\mathbf{M}_0\mathbf{e}\mathbf{e} ,\\ &\mathbf{V}_0=-2\mathbf{L}_0^{-1}\mathbf{M}_0\mathbf{e}\mathbf{e}^* .\end{aligned} \tag{17}$$

Substitution into (13) yields

$$\begin{aligned}\mathbf{B}_3^{(1)}=&-\left[\frac{\partial}{\partial\tau}-\chi\mathbf{L}_1\right]A\mathbf{e}\\ &+(2\mathbf{M}_0\mathbf{e}\mathbf{V}_0+2\mathbf{M}_0\mathbf{e}^*\mathbf{V}_++3\mathbf{N}_0\mathbf{e}\mathbf{e}\mathbf{e}^*)|A|^2A .\end{aligned}$$

Finally, the solvability condition (15) for $\nu=3$ takes the form of the Landau equation

$$N\frac{\partial A}{\partial\tau}=\chi\lambda A-gA|A|^2 , \tag{18}$$

where

$$\begin{aligned}&N=\mathbf{e}_L\cdot\mathbf{e} ,\\ &\lambda=\mathbf{e}_L\mathbf{L}_1\mathbf{e} ,\\ &g=-2\mathbf{e}_L\cdot(\mathbf{M}_0\mathbf{e}\mathbf{V}_0+\mathbf{M}_0\mathbf{e}^*\mathbf{V}_+)-3\mathbf{e}_L\cdot\mathbf{N}_0\mathbf{e}\mathbf{e}\mathbf{e}^* ,\end{aligned}$$

and $\mathbf{V}_0,\mathbf{V}_+$ are given by (17). $\mathbf{L}_1$ can be calculated from its definition $\mathbf{L}_1=d\mathbf{L}_0/dP_{\mathrm{CO}}$. So the elements in $\mathbf{L}_1$ are given by

$$(\mathbf{L}_1)_{ij}=\sum_{k=1}^{3}\frac{\partial^2f_i(\mathbf{Y}_0)}{\partial Y_{0j}\partial Y_{0k}}\frac{\partial Y_{0k}}{\partial P_{\mathrm{CO}}}+\frac{\partial\mathbf{L}_{ij}}{\partial P_{\mathrm{CO}}},\quad i,j=1,2,3 .$$

Note that had we kept the spatial dependence, there would have been a diffusion term ∂_X^2A with coefficient $d=\mathbf{e}_L\mathbf{D}\mathbf{e}$. Now, if $\mathrm{Re}g>0$, this equation predicts a supercritical bifurcation with new solutions existing whenever $\chi\mathrm{Re}\lambda>0$; for negative $\mathrm{Re}g$, the bifurcation is subcritical and $\chi\mathrm{Re}\lambda$ must be negative.

This amplitude equation represents the spatially uniform mode and thus is not connected to any standing-wave structure. Since in the absence of global coupling the $q=0$ mode is the most unstable (see Fig. 1), one might expect that the uniform state will be the selected structure. Nevertheless, let us continue and study the analogous amplitude equation for spatially nontrivial modes. To do this, we introduce an explicit spatial dependence in $\mathbf{u}_1$. Repeating the calculations, we have

$$\left[\frac{\partial}{\partial t}-\mathbf{D}\partial_x^2-\mathbf{L}_0\right]\mathbf{u}_\nu=\mathbf{B}_\nu,\quad \nu=1,2,3,\ldots . \tag{19}$$

The first few $\mathbf{B}_\nu$'s are

$$\begin{aligned}&\mathbf{B}_1=0 ,\\ &\mathbf{B}_2=\mathbf{M}_0\mathbf{u}_1\mathbf{u}_1 ,\\ &\mathbf{B}_3=-\left[\frac{\partial}{\partial\tau}-\chi\mathbf{L}_1\right]\mathbf{u}_1+2\mathbf{M}_0\mathbf{u}_1\mathbf{u}_2+\mathbf{N}_0\mathbf{u}_1\mathbf{u}_1\mathbf{u}_1 .\end{aligned} \tag{20}$$

For $\nu=1$, the homogeneous equation has the solution

$$\mathbf{u}_1=\mathbf{e}_q[A_R(\tau,X)e^{i(\omega_qt-qx)}+A_L(\tau,X)e^{i(\omega_qt+qx)}]+\mathrm{c.c.} ,$$

with $\mathbf{e}_q$ the eigenvector of $(\mathbf{L}_0-\mathbf{D}q^2)$ corresponding to the eigenvalue $i\omega_q$. One can easily check that when $|A_R|=|A_L|$, this will give a standing-wave pattern. If $A_R\neq0$, $A_L=0$ or $A_R=0$, $A_L\neq0$, traveling waves will arise.

Now $\mathbf{B}_\nu$ is decomposed as

$$\mathbf{B}_\nu=\sum_{l=-\infty}^{\infty}\sum_{m=-\infty}^{\infty}\mathbf{B}_\nu^{(l,m)}(\tau,X)e^{il\omega_qt}e^{imqx}$$

and solvability may be expressed as

$$\mathbf{e}_{qL}\cdot\mathbf{B}_\nu^{(1,\pm1)}(\tau,X)=0 . \tag{21}$$

Again, we find that only the third-order solvability condition gives nontrivial results. Since $\mathbf{u}_2$ is involved in $\mathbf{B}_3$, we have to solve $\mathbf{u}_2$ from Eq. (19) for $\nu=2$ first, with a form

$$\begin{aligned}\mathbf{u}_2=&\mathbf{V}_{+R}A_R^2e^{2i(\omega_qt-qx)}+\mathbf{V}_{+L}A_L^2e^{2i(\omega_qt+qx)}+\mathbf{V}_{-R}A_R^{*2}e^{-2i(\omega_qt-qx)}+\mathbf{V}_{-L}A_L^{*2}e^{-2i(\omega_qt+qx)}+\mathbf{V}_{+t}A_RA_Le^{2i\omega_qt}\\ &+\mathbf{V}_{-t}A_R^*A_L^*e^{-2i\omega_qt}+\mathbf{V}_{-x}A_RA_L^*e^{-2iqx}+V_{+x}A_R^*A_Le^{2iqx}+\mathbf{V}_{0R}|A_R|^2+\mathbf{V}_{0L}|A_L|^2 .\end{aligned} \tag{22}$$

By substituting Eq. (22) into (20) and the solvability condition for $\nu=3$, we obtain

$$\begin{aligned}&N_q\frac{\partial A_R}{\partial\tau}=\chi\lambda_qA_R-g_1A_R|A_R|^2-g_2A_R|A_L|^2 ,\\ &N_q\frac{\partial A_L}{\partial\tau}=\chi\lambda_qA_L-g_1A_L|A_L|^2-g_2A_L|A_R|^2 ,\end{aligned} \tag{23}$$

where

$$\begin{aligned}&N_q=\mathbf{e}_{qL}\cdot\mathbf{e}_q ,\\ &\lambda_q=\mathbf{e}_{qL}L_1\mathbf{e}_q ,\\ &g_1=-2\mathbf{e}_{qL}\cdot(\mathbf{M}_0\mathbf{e}_q\mathbf{V}_{0R}+\mathbf{M}_0\mathbf{e}_q^*\mathbf{V}_{+R})\\ &\quad-3\mathbf{e}_{qL}\cdot\mathbf{N}_0\mathbf{e}_q\mathbf{e}_q\mathbf{e}_q^*\\ &g_2=-2\mathbf{e}_{qL}\cdot(\mathbf{M}_0\mathbf{e}_q\mathbf{V}_{0R}+\mathbf{M}_0\mathbf{e}_q\mathbf{V}_{+x}+\mathbf{M}_0\mathbf{e}_q^*\mathbf{V}_{+t})\\ &\quad-6\mathbf{e}_{qL}\cdot\mathbf{N}_0\mathbf{e}_q\mathbf{e}_q\mathbf{e}_q^* .\end{aligned}$$

Here $\mathbf{V}_{+R}$, $\mathbf{V}_{0R}$, $\mathbf{V}_{+x}$, and $\mathbf{V}_{+t}$ can be calculated from Eq. (19) as mentioned above and their values are given below,

$$\mathbf{V}_{+R}=-(\mathbf{L}_0-4\mathbf{D}_q^2-2i\omega)^{-1}\mathbf{M}_0\mathbf{e}_q\mathbf{e}_q ,$$

$$\mathbf{V}_{0R}=-2\mathbf{L}_0^{-1}\mathbf{M}_0\mathbf{e}_q\mathbf{e}_q^* ,$$

$$\mathbf{V}_{+x}=-2(\mathbf{L}_0-4\mathbf{D}q^2)^{-1}\mathbf{M}_0\mathbf{e}_q\mathbf{e}_q^* ,$$

$$\mathbf{V}_{+t}=-2(\mathbf{L}_0-2i\omega)^{-1}\mathbf{M}_0\mathbf{e}_q\mathbf{e}_q .$$

Again, were we to include spatial modulation we would get the group-velocity term $-d_q\partial_X A_R$ or $+d_q\partial_X A_L$ in the two parts of Eq. (23), with

$$d_q=2iq\mathbf{e}_{qL}\mathbf{D}\mathbf{e}_q .$$

Now, the relevant system consists of two-coupled amplitude equations. Each amplitude equation is similar to Eq. (18) but with an additional cross-coupling term $g_2 A_R|A_L|^2$ (or $g_2 A_L|A_R|^2$). It is easy to check that when $q=0$, we have $g_1=g$, $N_q=N$, $\lambda_q=\lambda$, which implies consistency between Eq. (18) and Eq. (23). For simplicity, we will suppress the index q in N, λ, and d from later on.

We have calculated each of the coupling coefficients in Eq. (23) for different wave vectors q for some specific parameter choices ($T=540$ K, $P_{O_2}=4.7\times10^{-5}$ Torr) which will be maintained throughout this work. The results are shown in Figs. 2 and 3. We will return to a discussion of the solutions of this system in Sec. IV, after we discuss the modifications necessary in the presence of global coupling.

C. Amplitude equations with global couplings

The global-coupling terms which were ignored in the above calculations are expected to play an important role in forming standing waves. So the next step is to modify Eq. (23) by including the global-coupling effect. The actual values of the global couplings are not precisely known; we will for simplicity keep only α and β nonzero. This may not be the most physical assumption (since α' is probably significant), but will lead to the codimension-two situation discussed above. Let a bar denote a spatial average, i.e., $\bar{\mathbf{u}}=(1/L)\int \mathbf{u}\,dx$. Then obviously $\bar{\mathbf{Y}}_0=\mathbf{Y}_0$. Now the evolution functions F_i ($i=1,2,3$) depend not only on fields $\mathbf{Y}=(c,o,a)$ but also on their averages $\bar{\mathbf{Y}}=(\bar{c},\bar{o},\bar{a})$. So the dynamical Eq. (2) can be rewritten as

$$\frac{\partial\mathbf{Y}}{\partial t}=\mathbf{D}\partial_x^2\mathbf{Y}+\mathbf{F}(\mathbf{Y},\bar{\mathbf{Y}}) . \tag{24}$$

Note that F is a linear function of the $\bar{\mathbf{Y}}$. Again expanding about the Hopf-bifurcation point yields

$$\frac{\partial\mathbf{u}}{\partial t}=\mathbf{D}\partial_x^2\mathbf{u}+\mathbf{L}\mathbf{u}+\mathbf{L}'\bar{\mathbf{u}}+\mathbf{M}^{(1)}\mathbf{u}\mathbf{u}+2\mathbf{M}^{(2)}\mathbf{u}\bar{\mathbf{u}}+\mathbf{N}^{(1)}\mathbf{u}\mathbf{u}\mathbf{u}+3\mathbf{N}^{(2)}\mathbf{u}\mathbf{u}\bar{\mathbf{u}}+\cdots , \tag{25}$$

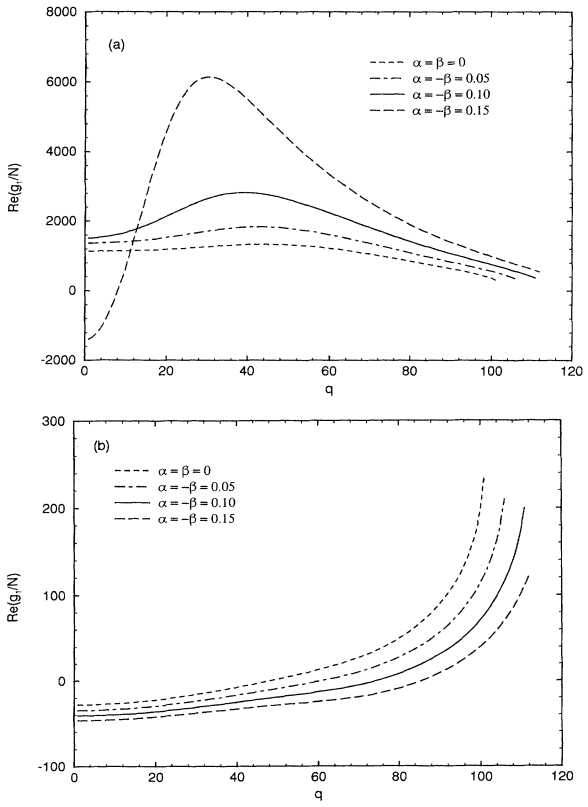

FIG. 2. $\mathrm{Re}(g_1/N)$ vs q with or without global couplings. There are two branch curves in each case, corresponding to different P_{CO}. (a) For larger P_{CO} and (b) for smaller P_{CO}.

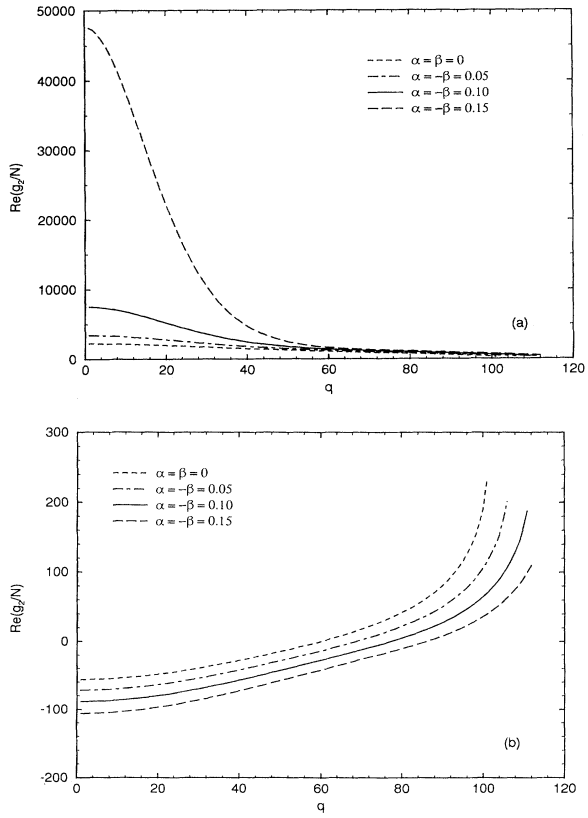

FIG. 3. $\mathrm{Re}(g_2/N)$ vs q with or without global couplings. (a) For larger P_{CO} and (b) for smaller P_{CO}.

where the new terms (as compared to the previous expansion) are

$$L'_{ij}=\frac{\partial F_i(\mathbf{Y}_0)}{\partial \bar{Y}_{0j}} ,$$

$$(\mathbf{M}^{(2)}\mathbf{u}\bar{\mathbf{u}})_i=\sum_{j,k}\frac{1}{2!}\frac{\partial^2 F_i(\mathbf{Y}_0)}{\partial Y_{0j}\partial \bar{Y}_{0k}}u_j\bar{u}_k , \tag{26}$$

$$(\mathbf{N}^{(2)}\mathbf{u}\mathbf{u}\bar{\mathbf{u}})_i=\sum_{j,k,l}\frac{1}{3!}\frac{\partial^3 F_i(\mathbf{Y}_0)}{\partial Y_{0j}\partial Y_{0k}\partial \bar{Y}_{0l}}u_j u_k\bar{u}_l .$$

Clearly, L_{ij}'s are the same in Sec. III B, and $\mathbf{M}^{(1)}\mathbf{u}\mathbf{u}=\mathbf{M}\mathbf{u}\mathbf{u}$, $\mathbf{N}^{(1)}\mathbf{u}\mathbf{u}\mathbf{u}=\mathbf{N}\mathbf{u}\mathbf{u}\mathbf{u}$. Proceeding as before, we obtain

$$\left[\frac{\partial}{\partial t}-\mathbf{D}\partial_x^2-\mathbf{L}_0\right]\mathbf{u}_\nu-\mathbf{L}'_0\bar{\mathbf{u}}_\nu=\mathbf{B}_\nu,\quad \nu=1,2,3,\ldots \tag{27}$$

where

$$\mathbf{B}_1=0 ,$$

$$\mathbf{B}_2=\mathbf{M}_0^{(1)}\mathbf{u}_1\mathbf{u}_1+2\mathbf{M}_0^{(2)}\mathbf{u}_1\bar{\mathbf{u}}_1 ,$$

$$\mathbf{B}_3=-\left[\frac{\partial}{\partial\tau}-\chi\mathbf{L}_1-2\mathbf{D}\partial_x\partial_X\right]\mathbf{u}_1-\chi\mathbf{L}'_1\bar{\mathbf{u}}_1$$
$$+2(\mathbf{M}_0^{(1)}\mathbf{u}_1\mathbf{u}_2+\mathbf{M}_0^{(2)}\mathbf{u}_1\bar{\mathbf{u}}_2+\mathbf{M}_0^{(2)}\mathbf{u}_2\bar{\mathbf{u}}_1)$$
$$+\mathbf{N}_0^{(1)}\mathbf{u}_1\mathbf{u}_1\mathbf{u}_1+3\mathbf{N}_0^{(2)}\mathbf{u}_1\mathbf{u}_1\bar{\mathbf{u}}_1 . \tag{28}$$

Let us first focus on the Hopf bifurcation itself, arising from the locus of points at which the homogeneous solutions of the $\nu=1$ piece of Eq. (27) neither grows nor decays. Because of the global-coupling term L'_0, the behavior of the $q=0$ mode is qualitatively different than that at finite q. This is immediately evident in Fig. 4; we have plotted the Hopf-bifurcation lines in the P_{CO}-P_{O_2} plane. We see that there are (two) codimension-two points at which the q mode and the zero mode go unstable together. Furthermore, there are regions in the parameter space for which the only instability is the spatially nonuniform structures; if we enter the oscillatory region through this part of the space, we naturally expect

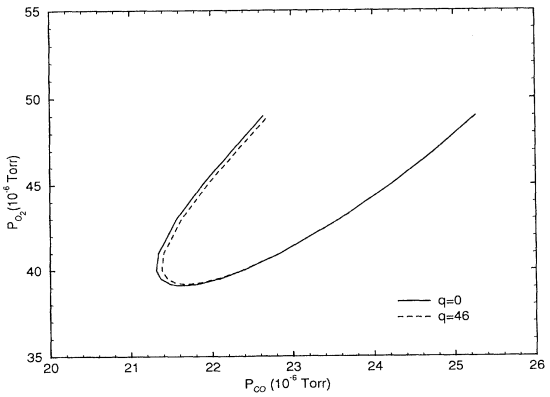

FIG. 4. Contours of the Hopf bifurcation with $\alpha=0.1$, $\beta=-0.1$.

to see waves instead of uniform oscillations.

We will proceed by considering three cases. First, if we are not near the codimension-two point, we can consider independently the amplitude equations for the zero and nonzero wave-vector modes. If we are close to such a point, we must include both amplitudes leading to a set of three-coupled amplitude equations. Finally, we consider separately the possibility of a resonance between the global oscillation and the finite wave-vector modes.

1. *Simple waves, $\bar{u}_1=0$*

We use the homogeneous solution

$$\mathbf{u}_1=\mathbf{e}_q[A_R(\tau,X)e^{i(\omega_q t-qx)}+A_L(\tau,X)e^{i(\omega_q t+qx)}]+\text{c.c.} \tag{29}$$

In this case, the solvability condition is the same as Eq. (21). By comparing Eq. (28) with Eq. (20), we observe that the $\mathbf{B}_2$'s are the same, while $\mathbf{B}_3$ is now altered by the addition of the term $2(\mathbf{M}_0^{(2)}\mathbf{u}_1\bar{\mathbf{u}}_2+\mathbf{M}_0^{(2)}\mathbf{u}_2\bar{\mathbf{u}}_1)$. Therefore, $\mathbf{u}_2$ has the same form as Eq. (22) and $\bar{\mathbf{u}}_2$ is given by

$$\bar{\mathbf{u}}_2=\mathbf{V}_{+t}A_R A_L e^{2i\omega_q t}+\mathbf{V}_{-t}A_R^* A_L^* e^{-2i\omega_q t}+\mathbf{V}_{0R}|A_R|^2$$
$$+\mathbf{V}_{0L}|A_L|^2 .$$

The coefficients in this expression for $\mathbf{u}_2$ are modified to be

$$\mathbf{V}_{0R}=-2(\mathbf{L}_0+\mathbf{L}'_0)^{-1}\mathbf{M}_0^{(1)}\mathbf{e}_q\mathbf{e}_q^* ,$$
$$\mathbf{V}_{+t}=-2(\mathbf{L}_0+\mathbf{L}'_0-2i\omega)^{-1}\mathbf{M}_0^{(1)}\mathbf{e}_q\mathbf{e}_q . \tag{30}$$

$\mathbf{V}_{+R}$ and $\mathbf{V}_{+x}$ are unchanged since they are determined by solving spatially nonuniform equations.

By repeating the derivation of Eq. (23), we find that the amplitude equations have the same form as Eq. (23) except that

$$g_1\to g_1-2\mathbf{e}_{qL}\cdot\mathbf{M}_0^{(2)}\mathbf{e}_q\mathbf{V}_{0R} ,$$
$$g_2\to g_2-2\mathbf{e}_{qL}\cdot(\mathbf{M}_0^{(2)}\mathbf{e}_q\mathbf{V}_{0R}+\mathbf{M}_0^{(2)}\mathbf{e}_q^*\mathbf{V}_{+t}) ,$$

and $\mathbf{V}_{+t}$, $\mathbf{V}_{0R}$ are modified as given in Eq. (30).

In summary, when the global gas-phase coupling is introduced, the amplitude equations are

$$N\frac{\partial A_R}{\partial\tau}=\chi\lambda A_R-d\partial_X A_R-g_1 A_R|A_R|^2-g_2 A_R|A_L|^2 ,$$
$$N\frac{\partial A_L}{\partial\tau}=\chi\lambda A_L+d\partial_X A_L-g_1 A_L|A_L|^2-g_2 A_L|A_R|^2 , \tag{31}$$

with

$$g_1=-2\mathbf{e}_{qL}\cdot(\mathbf{M}_0^{(1)}\mathbf{e}_q\mathbf{V}_{0R}+\mathbf{M}_0^{(1)}\mathbf{e}_q^*\mathbf{V}_{+R}+\mathbf{M}_0^{(2)}\mathbf{e}_q\mathbf{V}_{0R})$$
$$-3\mathbf{e}_{qL}\cdot\mathbf{N}_0^{(1)}\mathbf{e}_q\mathbf{e}_q\mathbf{e}_q^* ,$$
$$g_2=-2\mathbf{e}_{qL}\cdot(\mathbf{M}_0^{(1)}\mathbf{e}_q\mathbf{V}_{0R}+\mathbf{M}_0^{(1)}\mathbf{e}_q\mathbf{V}_{+x}+\mathbf{M}_0^{(1)}\mathbf{e}_q^*\mathbf{V}_{+t}$$
$$+\mathbf{M}_0^{(2)}\mathbf{e}_q\mathbf{V}_{0R}+\mathbf{M}_0^{(2)}\mathbf{e}_q^*\mathbf{V}_{+t})$$
$$-6\mathbf{e}_{qL}\cdot\mathbf{N}_0^{(1)}\mathbf{e}_q\mathbf{e}_q\mathbf{e}_q^* .$$

Obviously, when there is no global coupling, terms like

$\mathbf{M}_0^{(2)}\mathbf{uv}$ are zero, and we recover the results given previously.

We have calculated the coupling coefficients in Eq. (31) for different wave vectors. Graphs of $\mathrm{Re}(g_1/N)$ and $\mathrm{Re}(g_2/N)$ vs q for several different α and β are shown in Fig. 2 and Fig. 3. Since each q-mode Hopf bifurcation has two bifurcation points for fixed P_{O_2}, each curve consists of two branches, corresponding to larger and smaller P_{CO}, respectively. As q approaches its maximum value, the two branches come together since the two bifurcation points (P_{CO}, P_{O_2}) merge. We will show in the next section that standing waves cannot exist for the smaller P_{CO} branch. Along the top branch, varying α has only a minor effect as compared to varying β, perhaps accounting for the experimental observation that the relevant gas-phase coupling seems to be due to CO partial-pressure variations.

2. *Modulated waves*

The previous calculation looked at the ability of the system to support pure waves (either standing or traveling) at some spatial periodicity q. We will eventually argue that the waves seen in the experimental studies are actually modulated standing waves; by modulated, we mean that there are components of the concentration which have zero wave vector which are coupled to the basic wave at wave vector q. This corresponds in our formalism to solutions of Eq. (27) which have nonzero $\bar{\mathbf{u}}_1$. We now study the limitations on such a solution.

We make the ansatz

$$\mathbf{u}_1=\mathbf{e}_q[A_R(\tau,X)e^{i(\omega_q t-qx)}+A_L(\tau,X)e^{i(\omega_q t+qx)}]+\mathbf{e}_0 A_0(\tau,X)e^{i\omega_0 t}+\text{c.c.} \tag{32}$$

We now limit our calculation to the specific value of q for which the codimension-two point occurs at the (fixed) value of P_{O_2} we are considering; (actually there are two such values of q). We note that the only nonzero elements in $\mathbf{L}_0'$ are $(\mathbf{L}_0')_{12}$ and $(\mathbf{L}_0')_{12}$, with magnitudes much smaller than the corresponding elements in $\mathbf{L}_0$. Thus, $\omega_0\simeq\omega_q$, $\mathbf{e}_0\simeq\mathbf{e}_q$.

Now the new solvability conditions are

$$\begin{aligned}&\mathbf{e}_{qL}\cdot\mathbf{B}_\nu^{(\omega_q,\pm q)}(\tau,X)=0\ ,\\&\mathbf{e}_{0L}\cdot\mathbf{B}_\nu^{(\omega_0,0)}(\tau,X)=0\ ,\end{aligned} \tag{33}$$

where $\mathbf{B}_\nu^{(\omega_q,\pm q)}(\tau,X)$ and $\mathbf{B}_\nu^{(\omega_0,0)}(\tau,X)$ are the coefficients of $e^{i(\omega_q t\pm qx)}$ and $e^{i\omega_0 t}$ terms, respectively, and $\mathbf{e}_{qL}$ and $\mathbf{e}_{0L}$ are the left eigenvectors of $(\mathbf{L}_0-\mathbf{D}q^2)$ and $(\mathbf{L}_0+\mathbf{L}_0')$, respectively.

From symmetry considerations, we know that amplitude equations for A_R and A_L should be symmetric. Also, the coefficient of A_R-A_L coupling should be the same as that in Sec. III C1. So the only new coupling that enters can be found by considering the A_R-A_0 problem, namely, taking $A_L=0$.

Again, nontrivial results arise only from the solvability condition (33) to the third order, however also involving the $\mathbf{u}_2$ term. $\mathbf{u}_2$ has the form

$$\begin{aligned}\mathbf{u}_2=&\mathbf{V}_{+R}A_R^2e^{2i(\omega_q t-qx)}+\mathbf{V}_{-R}A_R^{*2}e^{-2i(\omega_q t-qx)}+\mathbf{V}_{0R}|A_R|^2+\mathbf{V}_{+0}A_0^2e^{2i\omega_0 t}+\mathbf{V}_{-0}A_0^{*2}e^{-2i\omega_0 t}+\mathbf{V}_0|A_0|^2\\&+\mathbf{V}_1A_RA_0e^{i(\omega_0+\omega_q)t-iqx}+\mathbf{V}_2A_R^*A_0^*e^{-i(\omega_0+\omega_q)t+iqx}+\mathbf{V}_3A_R^*A_0e^{i(\omega_0-\omega_q)t+iqx}+\mathbf{V}_4A_RA_0^*e^{i(\omega_q-\omega_0)t-iqx}\ .\end{aligned} \tag{34}$$

The unknowns $\mathbf{V}$'s in $\mathbf{u}_2$ can be determined from Eq. (27) and Eq. (28) with $\nu=2$. Then from the solvability conditions Eq. (33) with $\nu=3$, namely $\mathbf{e}_{qL}\cdot\mathbf{B}_3^{(\omega_q,-q)}(\tau,X)=0$, $\mathbf{e}_{0L}\cdot\mathbf{B}_3^{(\omega_0,0)}(\tau,X)=0$, we obtain the following evolution equation for the amplitudes:

$$\begin{aligned}N\frac{\partial A_R}{\partial\tau}&=\chi\lambda A_R-d\partial_X A_R-g_1A_R|A_R|^2-g_3A_R|A_0|^2\ ,\\N'\frac{\partial A_0}{\partial\tau}&=\chi(\lambda_1+\lambda_2)A_0-g_1'A_0|A_0|^2-g_3'A_0|A_R|^2\ ,\end{aligned} \tag{35}$$

where

$$N=\mathbf{e}_{qL}\cdot\mathbf{e}_q\ ,\quad N'=\mathbf{e}_{0L}\cdot\mathbf{e}_0\ ,\quad \lambda=\mathbf{e}_{qL}\mathbf{L}_1\mathbf{e}_q\ ,\quad \lambda_1=\mathbf{e}_{0L}\mathbf{L}_1\mathbf{e}_0\ ,\quad \lambda_2=\mathbf{e}_{0L}\mathbf{L}_1'\mathbf{e}_0\ ,$$

$$d=2iq\mathbf{e}_{qL}\mathbf{D}\mathbf{e}_q\ ,$$

$$g_1=-2\mathbf{e}_{qL}\cdot(\mathbf{M}_0^{(1)}\mathbf{e}_q\mathbf{V}_{0R}+\mathbf{M}_0^{(1)}\mathbf{e}_q^*\mathbf{V}_{+R}+\mathbf{M}_0^{(2)}\mathbf{e}_q\mathbf{V}_{0R})-3\mathbf{e}_{qL}\cdot\mathbf{N}_0^{(1)}\mathbf{e}_q\mathbf{e}_q\mathbf{e}_q^*\ ,$$

$$\begin{aligned}g_3=&-2\mathbf{e}_{qL}\cdot(\mathbf{M}_0^{(1)}\mathbf{e}_q\mathbf{V}_0+\mathbf{M}_0^{(1)}\mathbf{e}_q\mathbf{V}_4+\mathbf{M}_0^{(1)}\mathbf{e}_q^*\mathbf{V}_1+\mathbf{M}_0^{(2)}\mathbf{e}_q\mathbf{V}_0+\mathbf{M}_0^{(2)}\mathbf{V}_1\mathbf{e}_0^*+\mathbf{M}_0^{(2)}\mathbf{V}_4\mathbf{e}_0)\\&-6\mathbf{e}_{qL}\cdot(\mathbf{N}_0^{(1)}\mathbf{e}_q\mathbf{e}_0\mathbf{e}_0^*+\mathbf{N}_0^{(2)}\mathbf{e}_q\mathbf{e}_0\mathbf{e}_0^*+\mathbf{N}_0^{(2)}\mathbf{e}_q\mathbf{e}_0^*\mathbf{e}_0)\ ,\end{aligned}$$

$$\begin{aligned}g_1'=&-2\mathbf{e}_{0L}\cdot(\mathbf{M}_0^{(1)}\mathbf{e}_0\mathbf{V}_0+\mathbf{M}_0^{(1)}\mathbf{e}_0^*\mathbf{V}_{+0}+\mathbf{M}_0^{(2)}\mathbf{e}_0\mathbf{V}_0+\mathbf{M}_0^{(2)}\mathbf{V}_0\mathbf{e}_0+\mathbf{M}_0^{(2)}\mathbf{e}_0^*\mathbf{V}_{+0}+\mathbf{M}_0^{(2)}\mathbf{V}_{+0}\mathbf{e}_0^*)\\&-3\mathbf{e}_{0L}\cdot(\mathbf{N}_0^{(1)}\mathbf{e}_0\mathbf{e}_0\mathbf{e}_0^*+\mathbf{N}_0^{(2)}\mathbf{e}_0\mathbf{e}_0\mathbf{e}_0^*+2\mathbf{N}_0^{(2)}\mathbf{e}_0\mathbf{e}_0^*\mathbf{e}_0)\ ,\end{aligned}$$

$$g_3'=-2\mathbf{e}_{0L}\cdot(\mathbf{M}_0^{(1)}\mathbf{e}_0\mathbf{V}_{0R}+\mathbf{M}_0^{(1)}\mathbf{e}_q\mathbf{V}_3+\mathbf{M}_0^{(1)}\mathbf{e}_q^*\mathbf{V}_1+\mathbf{M}_0^{(2)}\mathbf{e}_0\mathbf{V}_{0R}+\mathbf{M}_0^{(2)}\mathbf{V}_{0R}\mathbf{e}_0)-6\mathbf{e}_{0L}\cdot(\mathbf{N}_0^{(1)}\mathbf{e}_q\mathbf{e}_q^*\mathbf{e}_0+\mathbf{N}_0^{(2)}\mathbf{e}_q\mathbf{e}_q^*\mathbf{e}_0)\ .$$

Note that the coupling g_3 and g_3' are not equal, representing the absence of any symmetry connecting the uniform mode with the q mode.

As mentioned before, the unknown **V**'s in the above expressions can be evaluated from Eq. (27) and Eq. (28) with $\nu=2$, i.e.,

$$\mathbf{V}_{+R}=-(\mathbf{L}_0-4\mathbf{D}q^2-2i\omega_q)^{-1}\mathbf{M}_0^{(1)}\mathbf{e}_q\mathbf{e}_q ,$$

$$\mathbf{V}_{0R}=-2(\mathbf{L}_0+\mathbf{L}_0')^{-1}\mathbf{M}_0^{(1)}\mathbf{e}_q\mathbf{e}_q^* ,$$

$$\mathbf{V}_{+0}=-(\mathbf{L}_0+\mathbf{L}_0'-2i\omega_0)^{-1}(\mathbf{M}_0^{(1)}\mathbf{e}_0\mathbf{e}_0+2\mathbf{M}_0^{(2)}\mathbf{e}_0\mathbf{e}_0) ,$$

$$\mathbf{V}_0=-2(\mathbf{L}_0+\mathbf{L}_0')^{-1}(\mathbf{M}_0^{(1)}\mathbf{e}_0\mathbf{e}_0^*+\mathbf{M}_0^{(2)}\mathbf{e}_0\mathbf{e}_0^*+\mathbf{M}_0^{(2)}\mathbf{e}_0^*\mathbf{e}_0) ,$$

$$\mathbf{V}_1=-2[\mathbf{L}_0-\mathbf{D}q^2-i(\omega_q+\omega_0)]^{-1}\times(\mathbf{M}_0^{(1)}\mathbf{e}_q\mathbf{e}_0+\mathbf{M}_0^{(2)}\mathbf{e}_q\mathbf{e}_0) ,$$

$$\mathbf{V}_3=-2[\mathbf{L}_0-\mathbf{D}q^2-i(\omega_0-\omega_q)]^{-1}\times(\mathbf{M}_0^{(1)}\mathbf{e}_q^*\mathbf{e}_0+\mathbf{M}_0^{(2)}\mathbf{e}_q^*\mathbf{e}_0) ,$$

$$V_4=-2[\mathbf{L}_0-\mathbf{D}q^2+i(\omega_0-\omega_q)]^{-1}\times(\mathbf{M}_0^{(1)}\mathbf{e}_q\mathbf{e}_0^*+\mathbf{M}_0^{(2)}\mathbf{e}_q\mathbf{e}_0^*) .$$

For $\beta=-\alpha$, the calculated values of q^* (the spatial wave vector at the codimension-two point), $\mathrm{Re}(g_1/N)$, $\mathrm{Re}(g_1'/N')$, $\mathrm{Re}(g_3/N)$, and $\mathrm{Re}(g_3'/N')$ vs α are shown in Figs. 5(a)–5(e). (Note that the codimension-two point occurs at a fixed wave vector since the only experimental parameter we allow to vary is P_{CO}.) Again, each curve has two branches, corresponding to larger and smaller P_{CO} with fixed P_{O_2}. The results show that when β is increased, namely when the global gas-phase coupling is more important, the real parts of the direct- and cross-coupling coefficients in the amplitude equations will increase on the larger P_{CO} branch. On the smaller P_{CO} branch, the coupling coefficients are always negative.

3. *Frequency degeneracy at the codimension-two point*

We now turn to the final possibility for a set of amplitude equations to describe our reaction-diffusion system. We first note that there is almost a coincidence between ω_0 and ω_q, the frequencies of the 0 and $q=q^*$ modes, for wave vectors in the range we are considering here. The frequency difference $\Delta\omega=(\omega_q-\omega_0)$ is $O(10^{-2}\omega_0)$ or less. The fact that this difference is so small suggests that there may be a new term in the amplitude equations corresponding to a parametric driving of the q modes by the global oscillation. Physically, this corresponds to a transfer of energy from the uniform oscillation to the

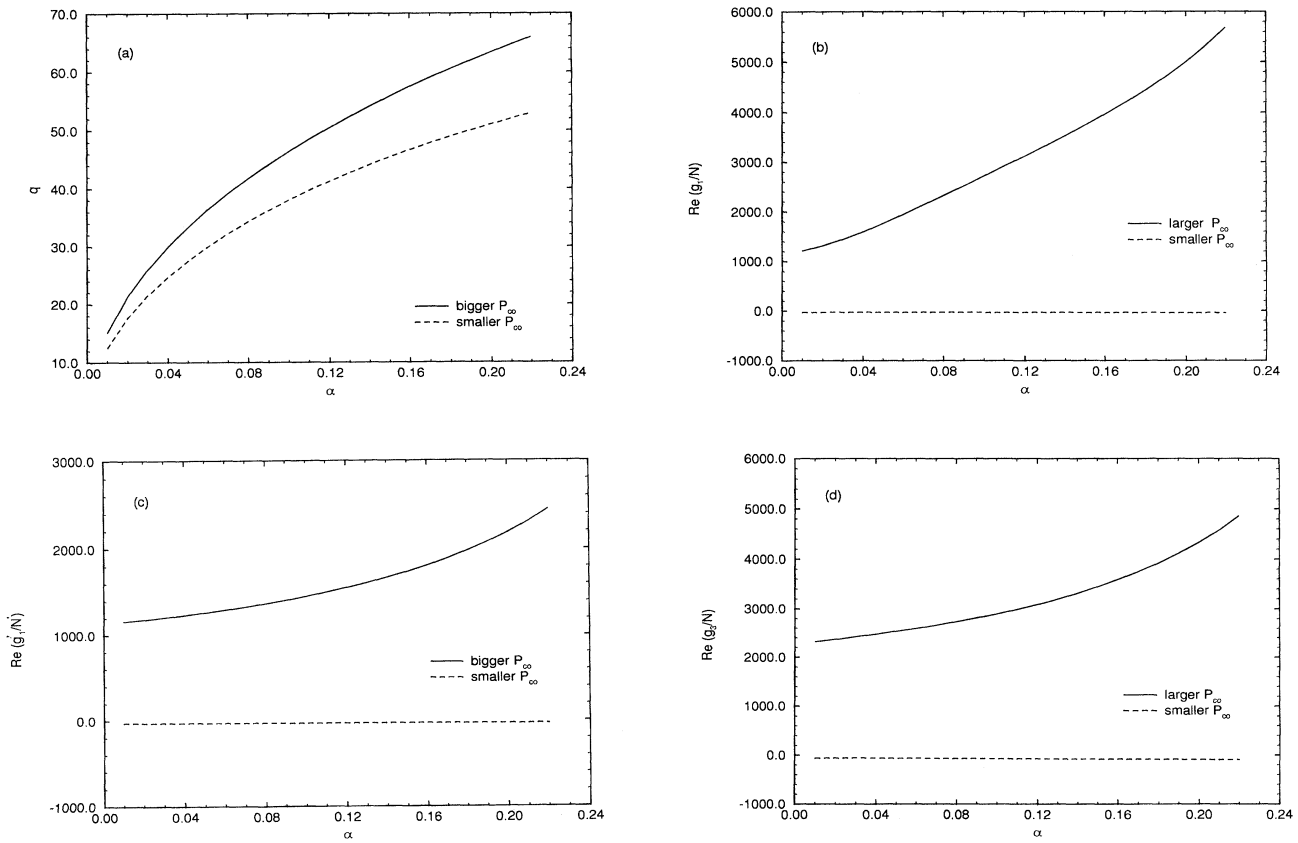

FIG. 5. Codimension-two wave vector (a) and coupling coefficients (b)–(e) vs α with $\beta=-\alpha$. (b) $\mathrm{Re}(g_1/N)$; (c) $\mathrm{Re}(g_1'/N')$; (d) $\mathrm{Re}(g_3/N)$; (e) $\mathrm{Re}(g_3'/N')$; (f) $\mathrm{Re}(g_4/N)$; (g) $\mathrm{Re}(g_4'/N')$.

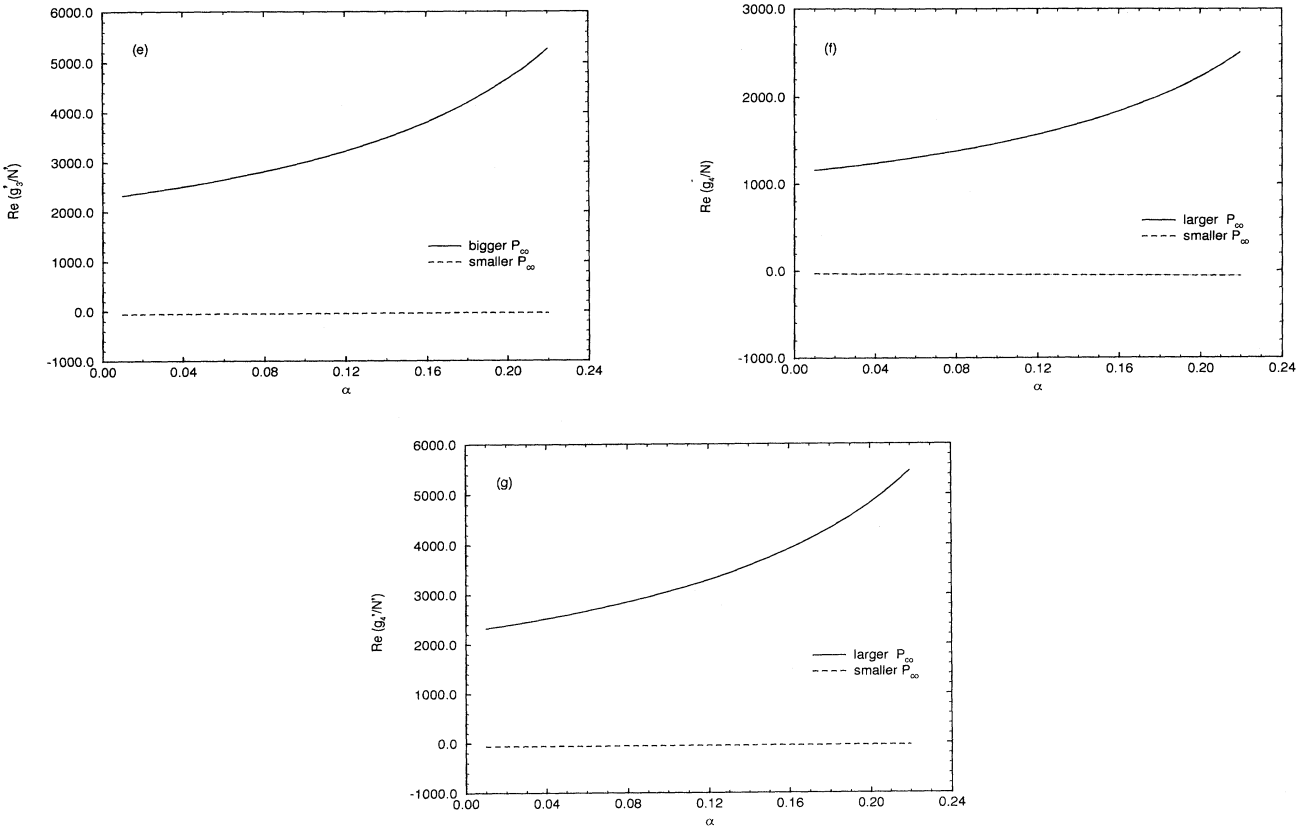

FIG. 5. (*Continued*).

standing wave via a resonant interaction.

For this situation, Eqs. (35) will be replaced by

$$N\frac{\partial A_R}{\partial \tau}=(\chi\lambda-iN\Delta\omega)A_R-g_1A_R|A_R|^2-g_2A_R|A_L|^2 -g_3A_R|A_0|^2-g_4A_L^*A_0^2 ,$$

$$N\frac{\partial A_L}{\partial \tau}=(\chi\lambda-iN\Delta\omega)A_L-g_1A_L|A_L|^2-g_2A_L|A_R|^2 -g_3A_L|A_0|^2-g_4A_R^*A_0^2 , \quad (36)$$

$$N'\frac{\partial A_0}{\partial \tau}=\chi(\lambda_1+\lambda_2)A_0-g_1'A_0|A_0|^2-g_3'A_0|A_R|^2 -g_3'A_0|A_L|^2-g_4'A_0^*A_RA_L ,$$

where the coefficients of the resonance terms g_4 and g_4' are given by

$$g_4=-2\mathbf{e}_{qL}\cdot(\mathbf{M}_0^{(1)}\mathbf{e}_q^*\mathbf{V}_{+0}+\mathbf{M}_0^{(1)}\mathbf{e}_0\mathbf{V}_3+\mathbf{M}_0^{(2)}\mathbf{e}_q^*\mathbf{V}_{+0} +\mathbf{M}_0^{(2)}\mathbf{V}_3\mathbf{e}_0) -3\mathbf{e}_{qL}\cdot(\mathbf{N}_0^{(1)}\mathbf{e}_q^*\mathbf{e}_0\mathbf{e}_0+2\mathbf{N}_0^{(2)}\mathbf{e}_q^*\mathbf{e}_0\mathbf{e}_0) ,$$

$$g_4'=-2\mathbf{e}_{0L}\cdot(\mathbf{M}_0^{(1)}\mathbf{e}_0^*\mathbf{V}_{RL}+\mathbf{M}_0^{(1)}\mathbf{e}_q\mathbf{V}_4+\mathbf{M}_0^{(2)}\mathbf{e}_0^*\mathbf{V}_{RL} +\mathbf{M}_0^{(2)}\mathbf{V}_{RL}\mathbf{e}_0^*) -2\mathbf{e}_{0L}\cdot(2\mathbf{N}_0^{(1)}\mathbf{e}_0^*\mathbf{e}_q\mathbf{e}_q+3\mathbf{N}_0^{(2)}\mathbf{e}_q\mathbf{e}_q\mathbf{e}_0^*) ,$$

with $\mathbf{V}_{RL}=-2(\mathbf{L}_0+\mathbf{L}_0'-2i\omega_q)^{-1}\mathbf{M}_0^{(1)}\mathbf{e}_q\mathbf{e}_q$. Actually $\Delta\omega$ is so small that it will be omitted in future calculations. Again for the special case of $\alpha=-\beta$, the values of $\mathrm{Re}(g_4/N)$ and $\mathrm{Re}(g_4'/N')$ vs α are given in Figs. 5(f) and 5(g).

In the next section, we turn to the implications of our variety of amplitude equations. We will propose that the experimentally observed standing-wave states are most closely described by including the parametric driving term given in the frequency-degenerate case.

IV. SPATIAL PATTERNS

A. Standing versus traveling waves

So far, we have obtained coupled equations governing small-amplitude oscillations near the Hopf-bifurcation point. There are two important types of solutions to these amplitude equations. When $A_R\neq 0$, $A_L=0$ or $A_R=0$, $A_L\neq 0$, we have traveling waves; when $|A_R|=|A_L|$, the solutions are standing waves. Note, however, that no traveling waves are seen in the experiments. In this section we calculate the stability of traveling- and standing-wave solutions so as to determine which solution is selected. We will not consider perturbations corresponding to small wave-vector shifts of the underlying pattern (phase perturbuations) and so we will drop the spatial-derivative terms in the remainder of this

work.

Let us first focus on the simple amplitude equations arising from just considering the two traveling waves, Eq. (31). It is easy to see that the selection of traveling- or standing-wave patterns is crucially affected by the competition between the direct-coupling term $A_R|A_R|^2$ (or $A_L|A_L|^2$) and the cross-coupling term $A_R|A_L|^2$ (or $A_L|A_R|^2$). First, we will consider the stability of the standing-wave pattern and set $A_L=A_R$. From (31), the solution in this case is $A_R=ae^{i(\Omega_S\tau+\phi)}$, where

$$a\equiv\left[\frac{\chi\mathrm{Re}\lambda}{\mathrm{Re}(g_1+g_2)}\right]^{1/2},$$

$$\Omega_S\equiv\chi\mathrm{Im}\lambda-\chi\mathrm{Re}\lambda\frac{\mathrm{Im}(g_1+g_2)}{\mathrm{Re}(g_1+g_2)},$$

and the phase ϕ can be set equal to zero by a shift of the origin on the x axis. Here N has been rescaled to one. Obviously, if $\mathrm{Re}(g_1+g_2)>0$, $\chi\mathrm{Re}\lambda$ must be positive, and this is a supercritical bifurcation. Otherwise, if $\mathrm{Re}(g_1+g_2)<0$, $\chi\mathrm{Re}\lambda$ should be negative, and this is a subcritical bifurcation.

Consider a small perturbation to the standing-wave solution, namely, $A_R=ae^{i\Omega_S\tau}+\delta A_R$, $A_L=ae^{i\Omega_S\tau}+\delta A_L$. Then we can linearize the amplitude equation (31),

$$\partial_\tau\delta A_R=\chi\lambda\delta A_R-2g_1a^2\delta A_R-g_1a^2e^{2i\Omega_S\tau}\delta A_R^*-g_2a^2\delta A_R-g_2a^2\delta A_L-g_2a^2e^{2i\Omega_S\tau}\delta A_L^*,$$

$$\partial_\tau\delta A_L=\chi\lambda\delta A_L-2g_1a^2\delta A_L-g_1a^2e^{2i\Omega_S\tau}\delta A_L^*-g_2a^2\delta A_R-g_2a^2\delta A_R-g_2a^2e^{2i\Omega_S\tau}\delta A_R^*.$$

After some calculations, we obtain two eigenmodes $\delta A_R=\pm\delta A_L=\pm\tilde{A}e^{(\sigma+i\Omega_S)\tau+i\gamma}$ and the corresponding eigenvalues are

$$\sigma=-\chi\mathrm{Re}\lambda[1+\cos(2\gamma)]\left[1+\left[\frac{\mathrm{Im}(g_2+g_1)}{\mathrm{Re}(g_2+g_1)}\right]^2\right]$$

and

$$\sigma=\chi\mathrm{Re}\lambda[(1+\cos(2\gamma)]\frac{\mathrm{Re}(g_2-g_1)}{\mathrm{Re}(g_2+g_1)}\times\left[1+\left[\frac{\mathrm{Im}(g_2-g_1)}{\mathrm{Re}(g_2-g_1)}\right]^2\right],$$

where γ's are given by

$$\sin(2\gamma)=\frac{\mathrm{Im}(g_2\pm g_1)}{\mathrm{Re}(g_2\pm g_1)}[1+\cos(2\gamma)].$$

Therefore, $\chi\mathrm{Re}\lambda$, $\mathrm{Re}(g_1+g_2)$, and $\mathrm{Re}(g_1-g_2)$ must be positive for the standing wave to exist and be stable. On the $(\mathrm{Reg}_1,\mathrm{Reg}_2)$ plane, this is illustrated in Fig. 6(a).

On the other hand, the stability of the traveling-wave solution can be calculated as follows. Take $A_R=0$, $A_L\neq0$ as an example. Then from Eq. (31), $A_L=be^{i(\Omega_T\tau+\phi)}$, where $b\equiv[(\chi\mathrm{Re}\lambda)/(\mathrm{Reg}_1)]^{1/2}$, $\Omega_T\equiv\chi\mathrm{Im}\lambda-\chi\mathrm{Re}\lambda[(\mathrm{Img}_1)/(\mathrm{Reg}_1)]$, and the phase ϕ can be set to zero by spatial translation. We introduce small perturbations δA_R and δA_L. Linearization of Eq. (31) around this solution gives

$$\partial_\tau A_R=\chi\lambda\delta A_R-g_2b^2\delta A_R,$$

$$\partial_\tau A_L=\chi\lambda\delta A_L-2g_1b^2\delta A_L-g_1b^2e^{2i\Omega_T\tau}\delta A_L^*.$$

In these two equations, δA_R and δA_L are decoupled. So the eigenmodes of δA_R and δA_L can be solved independently. From the first equation, the real part of the eigenvalue is $\chi\mathrm{Re}\lambda\{[\mathrm{Re}(g_1-g_2)]/\mathrm{Reg}_1\}$, which must thus be negative for the traveling wave to be stable. From the second equation, the eigenmode of δA_L is proportional to $e^{(\sigma+i\Omega_T)\tau+i\gamma}$, with

$$\sin(2\gamma)=\frac{\mathrm{Img}_1}{\mathrm{Reg}_1}[1+\cos(2\gamma)]$$

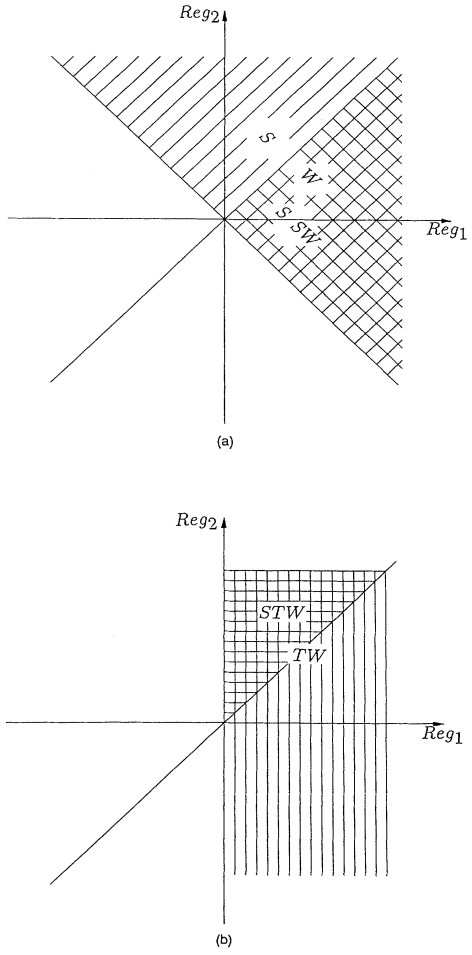

FIG. 6. Illustration of the linear stability of wave patterns in the $(\mathrm{Reg}_1,\mathrm{Reg}_2)$ plane: (a) standing waves, with SW (SSW) denoting (stable) standing waves; (b) traveling waves, with TW (STW) for (stable) traveling waves.

and

$$\sigma = -\chi \mathrm{Re}\lambda[1+\cos(2\gamma)]\left[1+\left[\frac{\mathrm{Im}g_1}{\mathrm{Re}g_1}\right]^2\right].$$

Thus the condition for stable traveling waves is that $\chi \mathrm{Re}\lambda > 0$, $\mathrm{Re}g_1 > 0$, and $\mathrm{Re}(g_1 - g_2) < 0$. On the $(\mathrm{Re}g_1, \mathrm{Re}g_2)$ plane, this is illustrated in Fig. 6(b).

Curves of $\mathrm{Re}(g_1 - g_2)$ and $\mathrm{Re}(g_1 + g_2)$ are given in Figs. 7 and 8. On the larger P_{CO} branch, we see that at large q, standing waves are selected as compared to traveling waves. This leads us to expect that one should observe standing waves on the upper branch. This prediction is consistent with the experiments [10] in the sense that the observed standing waves do indeed have small wavelength. One can also see that $\mathrm{Re}(g_1 - g_2)$ will increase as $|\beta|$ increases for large enough q, which implies that the introduction of the global coupling will enhance the stability of the standing-wave patterns. However, the amplitude of the standing wave $(\chi \mathrm{Re}\lambda)/[\mathrm{Re}(g_1 + g_2)]$ will decrease as $|\beta|$ increases. We have thus demonstrated that pure q-mode standing waves might be possible for some range of system parameters. On the lower P_{CO} branch, stable traveling waves are not possible since $\mathrm{Re}(g_1 - g_2)$ is always positive. Furthermore, $\mathrm{Re}(g_1 + g_2)$ is negative except for relatively large q as compared with the value expected for the codimension-two wave vector q^*. Since there will be no crossing of the Hopf-bifurcation contours, the standing wave would immediately decay to a pure global oscillation.

To recap, we have shown that the nonlinear selected wave for the q-mode Hopf bifurcation is a standing wave. The selection seems to be independent of the existence of the global coupling which only makes a quantitative difference in the values of the relevant coefficients. We do wish to stress again that without global coupling, one would expect that the global oscillation would bifurcate first and remain stable, quenching any q-mode instability. With the global coupling, this is not possible, due to the crossing of the Hopf-bifurcation contours.

However, we feel that a theory based on a pure q-mode solution is probably not relevant for the actual experimental results upon which our work is based. Such a theory would predict a predominance of the global oscillatory behavior with only a negligibly small region in parameter space for allowed standing waves; in fact, for nonzero positive values of α', this region may not exist at all. Instead, the standing waves seem to be observed in at least some finite range of parameters. There must be some additional mechanism for direct destabilization of globally synchronized behavior as compared to a finite wave-vector structure. We will now explain how this happens automatically if we impose the idea of frequency degeneracy on the codimension-two bifurcation analysis.

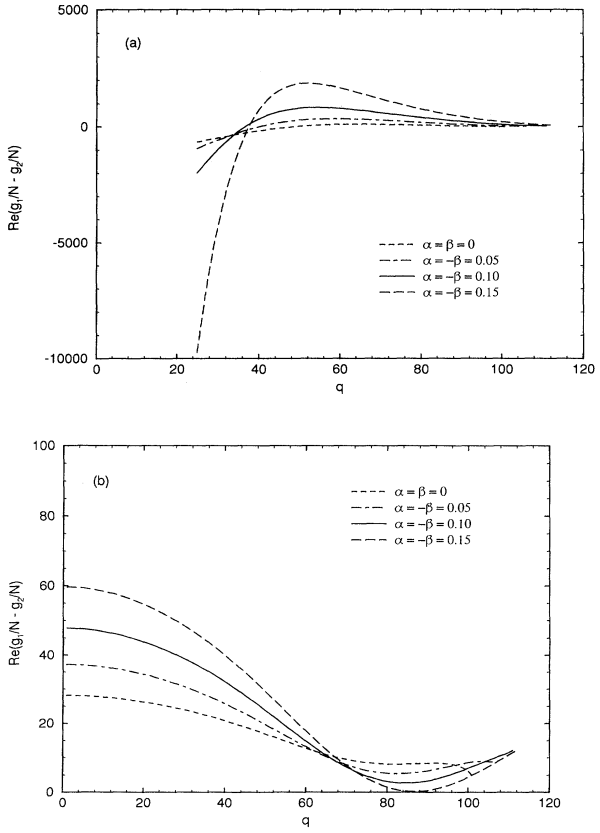

FIG. 7. $\mathrm{Re}[(g_1 - g_2)/N]$ vs q with or without global couplings. (a) For larger P_{CO} and (b) for smaller P_{CO}.

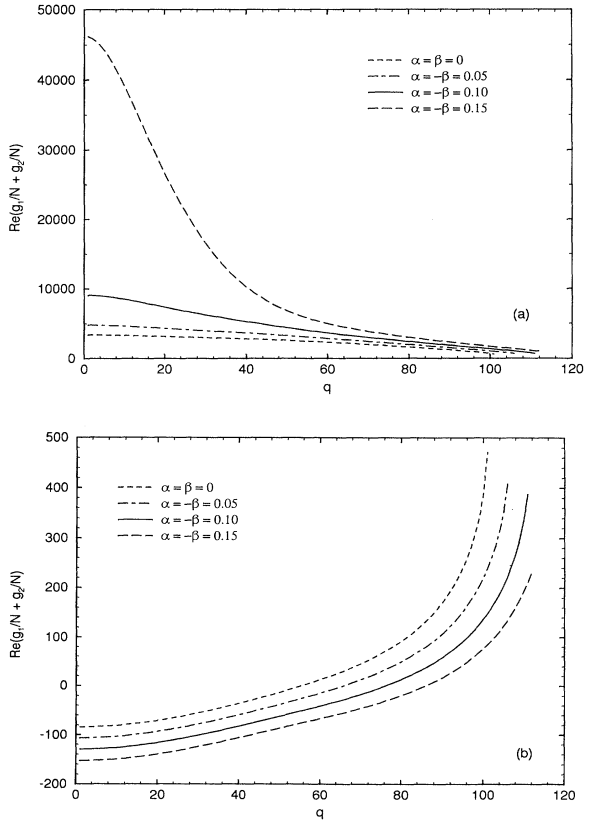

FIG. 8. $\mathrm{Re}(g_1 + g_2/N)$ vs q with or without global couplings. (a) For larger P_{CO} and (b) for smaller P_{CO}.

B. Self-induced parametric resonance

Now let us examine the importance of the presence of the self-induced parametric driving terms in the amplitude equations (36). First of all, these terms disallow modulated traveling-wave states; this is simply due to the fact that the global coupling terms couple left-going and right-going waves. This is of course consistent with the experimental findings. Second, the parametric resonance allows for the existence of the modulated standing waves where the global average coverages and the coverages at wave vector q synchronously oscillate. To investigate this possibility, we first consider the stability of a global oscillation $A_0=ce^{i\Omega_0\tau}$, $A_R=A_L=0$, with $c\equiv[[\chi\mathrm{Re}(\lambda_1+\lambda_2)]/\mathrm{Re}g_1']^{1/2}$, and $\Omega_0=\mathrm{Im}(\lambda_1+\lambda_2)-c^2\mathrm{Im}g_1'$. Assuming a perturbation $\delta A_L=\delta A_R=\tilde{A}_R e^{\sigma_R\tau+i\gamma_R}$, $\delta A_0=\tilde{A}_0 e^{\sigma_0\tau+i\gamma_0}$, we find the stability condition

$$\chi\mathrm{Re}\lambda-c^2[\mathrm{Re}g_3+\mathrm{Re}g_4\cos(2\gamma)+\mathrm{Im}g_4\sin(2\gamma)]<0\ ,$$

where the phase γ is determined by

$$c^2[\mathrm{Re}g_4\sin(2\gamma)-\mathrm{Im}g_4\cos(2\gamma)]$$
$$=\chi\mathrm{Im}(\lambda_1+\lambda_2)-\chi\mathrm{Im}\lambda+c^2(\mathrm{Im}g_3-\mathrm{Im}g_1')\ .$$

All of the relevant coefficients have been given in Figs. 5; the specific values these take at $\alpha=-\beta=0.1$ (for which case the codimension-two point is at $P_{\mathrm{CO}}=2.48\times10^{-5}$ Torr), are given in Table II. Evaluating this expression in the direction of decreasing P_{CO}, we find that $\mathrm{Re}\lambda\simeq\mathrm{Re}(\lambda_1+\lambda_2)$ and $\mathrm{Im}\lambda\simeq\mathrm{Im}(\lambda_1+\lambda_2)$, and the global mode is in fact unstable. This occurs because the phase γ is adjusted to make $\mathrm{Re}(g_4e^{-2i\gamma})<0$ and hence the global oscillation pumps energy into the standing wave.

Alternatively, one might consider the stability of a pure standing-wave solution $A_0=0$, $A_R=A_L=ae^{i\Omega_S\tau}$, with a and Ω_S given in Sec. V A. With the same perturbation form, linearization of equations (37) gives the stability condition

$$\chi\mathrm{Re}(\lambda_1+\lambda_2)-a^2(2\mathrm{Re}g_3'+\mathrm{Re}g_4'\cos(2\gamma)$$
$$+\mathrm{Im}g_4'\sin(2\gamma)]<0\ ,$$

where γ is found by solving

$$a^2[\mathrm{Re}g_4'\sin(2\gamma)-\mathrm{Im}g_4'\cos(2\gamma)]$$
$$=\chi\mathrm{Im}\lambda-\chi\mathrm{Im}(\lambda_1+\lambda_2)+a^2[2\mathrm{Im}g_3'-\mathrm{Im}(g_1+g_2)]\ .$$

Again, evaluating near $\mathrm{Re}\lambda\simeq\mathrm{Re}(\lambda_1+\lambda_2)$, we find that the pure standing-wave mode is also unstable.

The conditions embodied by the above stability criteria are shown schematically in Fig. 9; here we have presented the possible patterns as a function of $\chi\mathrm{Re}\lambda$ and $\chi\mathrm{Re}(\lambda_1+\lambda_2)$, the two unfolding parameters of the codimension-two bifurcation. As per the previous discussions, there is a region in the unfolding plane in which neither uniform oscillations nor a pure-q wave would be stable. Instead we find a modulated standing wave with three nonzero amplitudes. Assuming that $A_L=A_R=\mu e^{i\Omega\tau}$ and $A_0=\nu e^{i\Omega\tau}e^{i\gamma}$, we derive

$$\chi\lambda-(g_1+g_2)\mu^2-(g_3+g_4)\nu^2e^{2i\gamma}=i\Omega\ ,$$
$$\chi(\lambda_1+\lambda_2)-g_1'\nu^2-(2g_3'+g_4')\mu^2e^{-2i\gamma}=i\Omega\ ,$$

which can be directly solved to find μ^2 and ν^2. This is the stable solution in the aforementioned regime.

The modulated standing wave has one crucial characteristic that makes it attractive as a candidate for the experimentally discovered wave. The existence of this solution does not require that we carefully dial all the parameters so as to make the q-mode growth rate $\chi\mathrm{Re}\lambda$ larger than the global oscillation growth rate $\chi\mathrm{Re}(\lambda_1+\lambda_2)$. Instead, the condition is merely that the growth rates and frequencies are comparable, something which is much easier to arrange. We will see in the next section that one can indeed find stable modulated standing waves even for a set of parameters (for example, no global coupling whatsoever) for which the former possibility does not occur. For cases such as this, standard bifurcation analysis would predict stable global modes and it is only the parametric coupling which drives the nontrivial spatial structure.

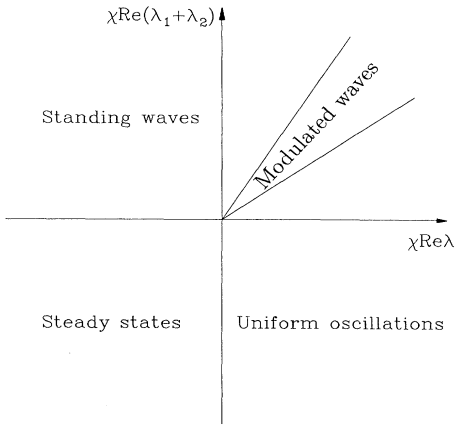

FIG. 9. Unfolding of the codimension-two bifurcation.

TABLE II. Amplitude equation parameters in sec^{-1} for $P_{\mathrm{CO}}=2.48\times10^{-5}$ Torr, $\alpha=-\beta=0.1$.

g_0	(1454.05, −7523.35)	g_q	(2723.57, −7116.96)
g_1	(3005.38, −14957.24)	g_1'	(2898.22, −14955.70)
g_3	(3057.19, −14928.53)	g_3'	(1469.11, −7461.73)
		g_2	(2013.51, −11959.55)

V. COMPUTER SIMULATIONS

In order to verify the above picture, we have performed direct numerical simulations of the model equations both with and without global-coupling terms. To do this we use a simple spatial grid with periodic boundary conditions (in a box of size L) and an explicit time-stepping scheme with time steps small enough for accurate and stable solutions [21]. We also choose values of q, P_{CO} so as to be in a regime where stable standing waves are expected.

The basic finding for $\alpha=-\beta=0.08$ is shown in Fig. 10

where we plot the evolution of the CO-concentration field and the average concentration fields $\bar{c}$, $\bar{o}$. The initial conditions are chosen by using a fixed q-mode perturbation on the steady-state concentrations. Clearly, there is both a standing-wave component (with wavelength $\lambda = L/2$, e.g., $L = 0.36$ mm implies $q = 2\pi/\lambda = 34.91$ mm^{-1}) as well as an overall, global oscillation (corresponding to $q = 0$ mode). This type of structure (modulated wave) is qualitatively similar to the standing-wave pattern observed in the catalysis experiments.

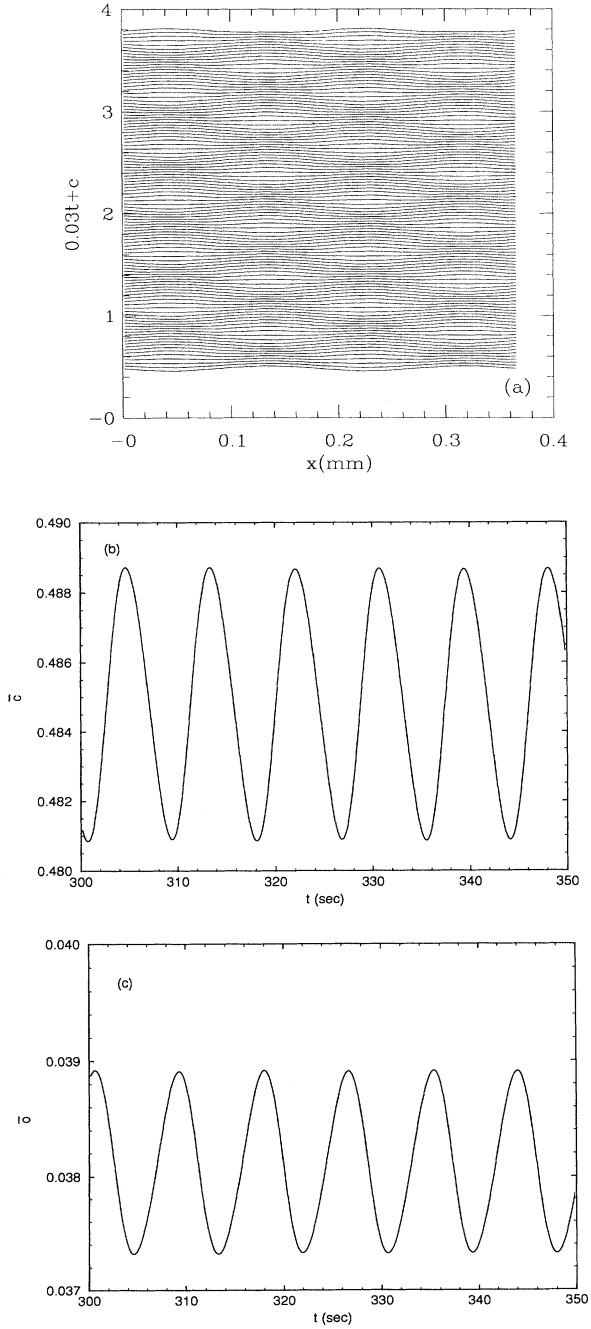

FIG. 10. (a) CO concentration profile evolving in time; here $P_{CO} = 2.46 \times 10^{-5}$ Torr, $q = 34.9$ mm^{-1}, $\alpha = 0.08$, $\beta = -0.08$. (b) and (c) Averages of CO and O coverages vs time.

In the previous example, the parameters were motivated by actually finding the relevant codimension-two point and the relevant modulated wave region. What is more surprising is that we can get modulated standing waves even without global couplings. For instance, in one run we set $P_{CO} = 2.41 \times 10^{-5}$ Torr and as always, $P_{O_2} = 4.70 \times 10^{-5}$ Torr. The wave vector is fixed by our box to equal 32.33 mm^{-1}, close to q^* at the codimension-two point for a relatively strong global coupling. We start the system with a random set of a, c, and

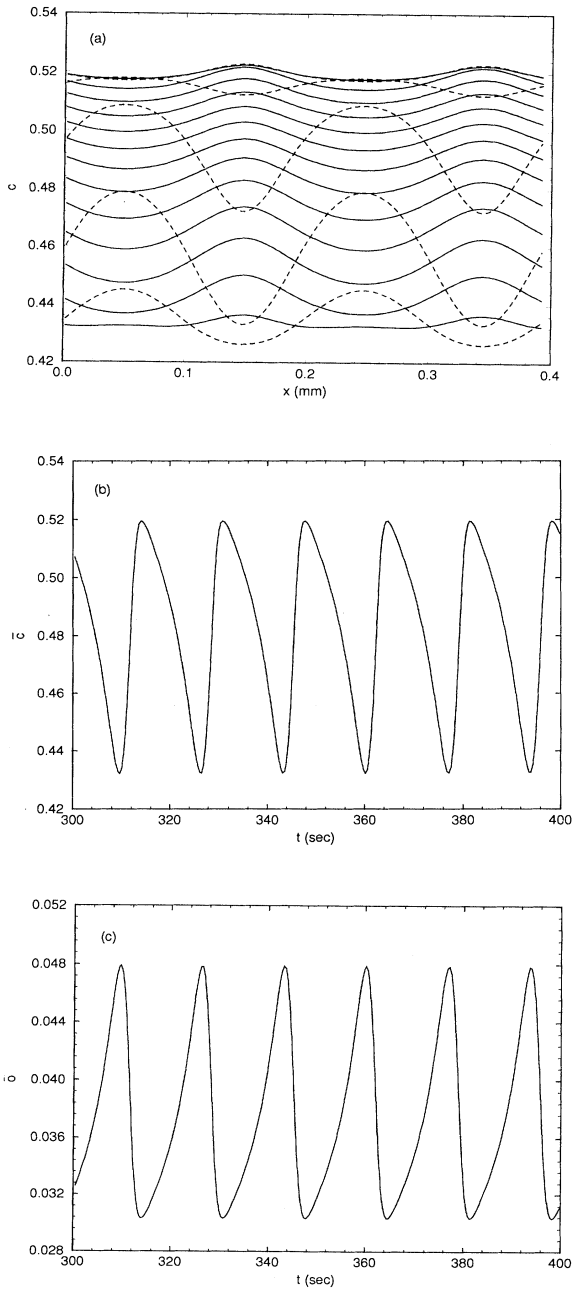

FIG. 11. (a) CO concentration profile evolving in time without global coupling; here $P_{CO} = 2.41 \times 10^{-5}$ Torr, $q = 32.2$ mm^{-1}. (b) and (c) Averages of CO and O coverages vs time.

o values near the (unstable) steady-state values. The CO concentration profile at late times and the evolution of $\bar{c}$, $\bar{o}$ with time are shown in Fig. 11. Again, there is a wave having both $q=0$ and $q\neq 0$ components. Note that the global oscillation in this case is stronger than that in the strong gas-phase couplings case, due to the fact that the linear growth rate of the global mode is larger than that of the standing-wave piece. In fact, even if we set $\alpha=\beta=0$, and have $\alpha'>0$, $\beta'<0$ (but not too large), we can still find stable wave states—here the global coupling is attempting to completely synchronize the surface oscillations, but is "overcome" by the parametric forcing.

Finally, we want to emphasize again the narrowness of the parameter range for which we expect to see (and do see in our simulations) standing waves. Although one could have searched directly via simulation for the standing-wave regime, the bifurcation analysis explains why this regime is so narrow and correctly predicts where to look.

VI. CONCLUSIONS

In this paper we have studied possible wave patterns in CO oxidation on a Pt(110) single-crystal surface. In particular, we have derived amplitude equations which determine the existence ranges and relative stability for standing waves and traveling waves; also, for the case of gas-phase coupling, we have studied the competition between uniform and spatially nonuniform oscillations. This was done within the framework of a model obtained by adding spatial transport to the reaction kinetic scheme of Eiswirth, Krischer, and Ertl.

Our results provide a first step towards a full understanding of the complex two-dimensional standing-wave spatial patterns seen experimentally. We do find stable (modulated) standing waves which qualitatively match those seen experimentally. The exact values of the parameters predicted by our calculations should, however, not be taken all that seriously since many of the fundamental rate constants are not known very precisely.

Several lines of investigation remain open for further exploration. Extension of our amplitude equations to include slowly varying spatial modulations might offer additional insight into the selection of the spatial wave vector. Also, extensions which would allow for two-dimensional effects such as dislocations are clearly necessary. Finally, the general problem of coupled oscillators with a global coupling is of interest for other systems, perhaps for interacting neural oscillators [22]. The generic behavior of such a system near a double Hopf bifurcation ($q=0$ and $q\neq 0$) is of course dependent only on the signs and relative magnitudes of the coupling coefficients and not on anything specific to the catalytic reaction dynamics.

ACKNOWLEDGMENTS

We would like to acknowledge M. Eiswirth, K. Krischer, and G. Ertl for explaining to us the details of the surface-reconstruction mechanism, H. Riecke for suggestions regarding the bifurcation theory, W.-J. Rappel for help in performing the simulations, and S. Yamamoto and C. Surko for useful discussions. This work is supported in part by the National Science Foundation under Grant No. DMR-9115413.

[1] *Oscillations and Traveling Waves in Chemical Systems,* edited by J. E. Field and M. Burger (Wiley, New York, 1985).
[2] R. Imbihl, M. P. Cox, G. Ertl, H. Müller, and W. Brenig, J. Chem. Phys. **83**, 1578 (1985).
[3] B. C. Sales, J. E. Turner, and M. B. Maple, Surf. Sci. **114**, 381 (1982).
[4] H. Levine and W. Reynolds, Phys. Rev. Lett. **66**, 2400 (1991).
[5] J. J. Tyson, and J. P. Keener, Physica D **32**, 327 (1988).
[6] For a recent review, see A. Winfree, Chaos **1**, 455 (1991).
[7] H. H. Rotermund, W. Engel, M. Kordesch, and G. Ertl, Nature **343**, 355 (1988).
[8] C. Surko and S. Yamamoto (private communication).
[9] H. Levine and X. Zou, J. Chem. Phys. **95**, 3815 (1991).
[10] S. Jakubith, H. H. Rotermund, W. Engel, A. von Oertzen, and G. Ertl, Phys. Rev. Lett. **65**, 3013 (1990).
[11] H. H. Rotermund, S. Jakubith, A. von Oertzen, and G. Ertl, Phys. Rev. Lett. **66**, 3083 (1991).
[12] H. H. Rotermund, W. Engel, S. Jakubith, A. von Oertzen, and G. Ertl, Ultramicroscopy **36**, 164 (1991).
[13] G. Ertl, Catalysis Lett. **9**, 219 (1991).
[14] R. M. Eiswirth, K. Krischer, and G. Ertl, Appl. Phys. A **51**, 79 (1990).
[15] K. Krischer, R. M. Eiswirth, and G. Ertl, Surf. Sci. **251**, 900 (1990).
[16] H. Levine and X. Zou, Phys. Rev. Lett. **69**, 204 (1992).
[17] S. Ladas, R. Imbihl, and G. Ertl, Surf. Sci. **198**, 42 (1988).
[18] R. M. Eiswirth, P. Möller, K. Wetzl, R. Imbihl, and G. Ertl, J. Chem. Phys. **90**, 510 (1989).
[19] Y. Kuramoto, *Chemical Oscillations, Waves and Turbulence* (Springer-Verlag, Berlin, 1984).
[20] H. Riecke and L. Kramer, J. Chem. Phys. **83**, 3941 (1985).
[21] W. H. Press *et al.*, *Numerical Recipes* (Cambridge University Press, Cambridge, England, 1990).
[22] See, e.g., *Methods in Neuronal Modeling,* edited by C. Koch and I. Segev (MIT, Cambridge, 1989).